Novel polyamide 6 nanocomposites with graphene oxide-modified silica

Regina Jeziórska[1), *)] (ORCID ID: 0000-0003-2518-6924), **Agnieszka Szadkowska[1)]** (0000-0003-3144-7422), **Ewa Spasówka-Kumosińska[1)]** (0000-0002-3827-2664), **Maciej Studziński[1)]** (0000-0002-7109-496X), **Magdalena Żubrowska[1)]** (0009-0006-7385-3647), **Magdalena Jurczyk-Kowalska[2)]** (0000-0002-2552-9408)

DOI: https://doi.org/10.14314/polimery.2024.11.6

Abstract: Graphene oxide-modified silica (GO-SiO_2) with particle sizes of 30 and 60 nm was obtained by sol-gel method and used as a hybrid nanofiller for polyamide 6. Maleic anhydride (MAH) was used to improve the interactions between the filler and the polymer matrix. The composites were obtained by extrusion. A constant amount of GO-SiO_2 (1 wt%) and MAH (0.5 wt%) was used. Photon correlation spectroscopy, SEM and low temperature nitrogen adsorption were used to characterize GO-SiO_2. The composites were evaluated by ATR-FT-IR, SEM, DSC, DMTA and TGA. The crystal structure, thermal properties, water absorption and mechanical properties were investigated. The results showed that GO-SiO_2 acts as a nucleating agent, increasing the crystallinity and crystallization temperature of the composites. In addition, GO-SiO_2 increased the stiffness of PA, with a greater effect for larger silica particles (60 nm). MAH slightly decreased stiffness and crystallinity but improved the tensile and impact properties because of the homogeneous dispersion of GO-SiO_2 in the polymer matrix, as well as improved interfacial interactions (SEM). Furthermore, the composites showed lower water absorption (by 30%) and higher thermal stability as evidenced by higher $T_{10\%}$ (1–6°C) and T_{max} (10–20°C).

Keywords: graphene oxide, silica, hybrid nanofiller, polyamide 6, thermal properties, mechanical properties.

Nowe nanokompozyty poliamidu 6 z krzemionką modyfikowaną tlenkiem grafenu

Streszczenie: Metodą zol-żel otrzymano krzemionkę modyfikowaną tlenkiem grafenu (GO-SiO_2) o wielkości cząstek 30 oraz 60 nm i zastosowano jako hybrydowy nanonapełniacz do poliamidu 6. Do poprawy oddziaływań między napełniaczem i osnową polimerową użyto bezwodnik maleinowy (MAH). Kompozyty otrzymano w procesie wytłaczania. Stosowano stałą ilość GO-SiO_2 (1%mas.) oraz MAH (0,5% mas.). Do scharakteryzowania GO-SiO_2 zastosowano spektroskopię korelacji fotonów, SEM i adsorpcję azotu w niskiej temperaturze. Kompozyty oceniono za pomocą ATR-FT-IR, SEM, DSC, DMTA i TGA. Zbadano strukturę krystaliczną, właściwości termiczne, absorpcję wody i właściwości mechaniczne. Wyniki pokazały, że GO-SiO_2 działa jako środek nukleujący, zwiększając krystaliczność i temperaturę krystalizacji kompozytów. Ponadto GO-SiO_2 zwiększyła sztywność PA, przy czym większy efekt uzyskano w przypadku większych cząstek krzemionki (60 nm). MAH nieznacznie zmniejszył sztywność i krystaliczność, ale poprawił właściwości mechaniczne przy rozciąganiu i udarność jako efekt homogenicznej dyspersji GO-SiO_2 w osnowie polimerowej, a także lepszych oddziaływań na granicy faz (SEM). Ponadto kompozyty wykazały mniejszą absorpcję wody (o 30%) i większą stabilność termiczną o czym świadczy wyższa $T_{10\%}$ (1–6°C) i T_{max} (10–20°C).

Słowa kluczowe: tlenek grafenu, krzemionka, hybrydowy napełniacz, poliamid 6, właściwości termiczne, właściwości mechaniczne.

Graphene oxide (GO) is an oxidized derivative of graphene, which can be widely used as an alternative or precursor to graphene due to its easy dispersibility and processability in aqueous medium [1]. GO is produced from graphite flakes by thermal oxidation method invented by Hummers and modified by his successors [2]. The

[1)] Łukasiewicz Research Network – Industrial Chemistry Institute, ul. Rydygiera 8, 01-793 Warszawa, Poland.

[2)] Warsaw University of Technology, Faculty of Materials Science and Engineering, ul. Wołoska 141, 02-507 Warszawa, Poland.

[*)] Author for correspondence: regina.jeziorska@ichp.lukasiewicz.gov.pl

resulting single atomic layers, like graphene, have many epoxy and hydroxyl groups on both sides of the basal carbon plane and carboxyl groups around their edges [3]. The carbon to oxygen ratio in graphene oxide is close to 2, and the surface coverage of oxidized areas can reach 60–70% [4]. The theoretical thickness of graphene oxide is in the range of 0.7–0.8 nm, twice that of pure graphene [4]. The actual thickness of graphene oxide flakes may be slightly larger due to surface contamination and organic adsorbates [4, 5]. Despite the lack of electrical advantages of graphene and slightly worse mechanical strength, graphene oxide and derivatives still show enormous potential in nanocomposite technology due to their exceptional mechanical properties, high flexibility, high binding potential and extremely high surface-to-volume ratio. The elastic modulus of a single graphene oxide sheet reaches up to 250 GPa, despite a considerable number of local defects, and is much higher than that of most known fillers [3]. Graphene oxide flakes are negatively charged under weakly acidic and alkaline conditions due to the presence of carboxyl groups. The zeta potential of graphene oxide decreases at higher pH values and can be as low as –50 mV at pH = 10.5 [6]. Graphene oxide does not precipitate from most polar solvents and can be incorporated into an appropriately charged polyelectrolyte matrix [1, 4].

Interactions between polymers and graphene-based materials play a key role in nanocomposite cohesion and its mechanical properties. Due to the homogeneous composition of graphene without other heteroatoms, molecular interactions with polymers are limited to weak van der Waals forces, hydrophobic–hydrophobic interactions, and π–π electrons [7]. Van der Waals forces are attractive forces generated by transient or permanent molecular dipoles. Although very weak, they contribute significantly to the bonding between graphene and polymers such as polyethylene due to its exceptionally large specific surface area [8]. Hydrophobic–hydrophobic interactions are a common way of graphene bonding in hydrophobic polymer matrices. The case of π–π electron interactions occurs in the presence of aromatic rings (polystyrene), which can form strong bonds [9, 10]. Graphene oxide has polar oxygen-containing functional groups such as epoxy, carbonyl, hydroxyl, and carboxyl [11]. Hydrogen bonding between polar donors and acceptor groups is common for graphene oxide. Epoxy, hydroxyl, carbonyl, and carboxyl groups on graphene oxide are highly polarized (negative charge on oxygen atom) [10]. As a result, graphene oxide can bond with various polar polymers, especially polyelectrolytes and proteins, through a network of hydrogen bonds and polar interactions [12]. Due to the high density and polarity of functional groups, the interfacial strength of polymer–graphene nanocomposites with hydrogen bond network can be overall higher than that of covalently cross-linked nanocomposites. The hardness of hydrogen bonded nanocomposites is significantly improved due to the ability to form in situ bonds, which is another advantage over the permanent nature of covalent cross-linking [5]. Covalent grafting of polymer chains onto the graphene oxide surface can ensure its better dispersion in the polymer matrix [13]. The mechanical strength of covalent bonds is the highest among intermolecular interactions. Hydroxyl-terminated polymers can cross-link graphene oxide layers by esterification of their carboxyl groups. Electrostatic interactions also play a key role in the bonding of graphene oxide with polar functional groups. Due to the strong electrostatic interactions and the reversibility of these interactions, nanocomposites are stiffer and harder than their counterparts without filler [4].

The properties of polymer nanocomposites based on graphene are significantly dependent on the specific surface area, aspect ratio, dispersion and content of graphene and the interaction at the interface [14–16]. The most crucial factor, along with the increase of the specific interfacial area, is the control of stress transfer across the interface, which can be achieved by covalent bonds, electrostatic interactions, hydrogen bonding or van der Waals interactions [17]. Fine dispersion of the reinforcement results in the formation of a large, specific interfacial area. Poor dispersion and aggregation of nanomaterials in the polymer matrix reduces the interfacial area and weakens the interfaces, leading to poor mechanical properties. Theoretically, it is not possible to achieve complete stress transfer across the interface, but a strong interface with efficient stress transfer is necessary to maximize mechanical strength [18]. Graphene derivatives are mechanically strong but also flexible, which makes them an ideal nanofiller to produce high-performance, multifunctional polymer nanocomposites [19]. Graphene oxide incorporated into the polymer matrix can significantly improve mechanical properties such as modulus, tensile and flexural strength, elongation, and hardness. High dispersion and appropriate interfacial interactions play a key role here.

Melt mixing is a practical approach that can be applied to polymer–graphene nanocomposites. However, heating, and high local mechanical stresses can affect the stability of the components, the shape of the flakes, and the reduction state of the graphene oxide sheets.

Melt blending has been used to prepare GO nanocomposites with polylactic acid (PLA) [20] and polyethylene terephthalate (PET) [21], PA [22] and EPDM elastomers [23]. The extrusion process promotes exfoliation of reduced graphene oxide in the case of isotactic polypropylene (iPP), poly(styrene–*co*–acrylonitrile) (SAN), polyamide 6 (PA6) and polycarbonate (PC), giving thermoplastic nanocomposites with homogeneously dispersed graphene material [24].

There are only a few examples of silica-graphene composites in scientific reports. GO-SiO_2 can combine the advantages of both materials. GO-SiO_2 systems have better properties compared to GO nanosheets and SiO_2 nanoparticles, which is attributed to the synergistic effect of both materials [25–27]. The introduction of GO-SiO_2

nanohybrids into the polymer coating reduces surface cracking and degradation under UV radiation as well increases its service life [28]. The corrosion protection efficiency (adhesion strength of epoxy coating to steel substrates and wetting angle) significantly increases after the addition of GO-SiO_2 nanohybrids.

Silane coupling agents are used to bind SiO_2 nanoparticles to GO surface, which leads to covalent bonding of GO active oxygen groups and SiO_2 hydroxyl groups SiO_2 [29, 30]. Ma *et al.* [26] studied the combination of 3-glycidoxypropyltrimethoxysilane functionalized GO with 3-aminopropyltriethoxysilane (APTS)-coated SiO_2. The reaction between silane coupling agents was used to prepare epoxy coatings containing 2 wt% SiO_2-GO. Ramezanzadeh *et* al. [31] obtained SiO_2-GO nanohybrids by a two-step sol-gel method using a mixture of tetraethoxy silane (TEOS) and APTS in water-alcohol solution. SiO_2-GO nanohybrids were obtained by hydrolysis and condensation reactions of TEOS precursor on GO sheets (interactions between hydroxyl groups of GO and hydroxyl groups of SiO_2) [32]. GO-SiO_2 nanohybrids were dispersed as nanofillers in solvent-based epoxy coatings. Addition of GO to PA 11 leads to a decrease in the coefficient of friction in dry sliding conditions, thus improving wear resistance and tribological properties of such composites [33, 34]. Pan *et al.* [35] observed an improvement in electrical conductivity as well as stiffness of nanocomposites based on graphite exfoliated with PA 6. Rehman *et al*. [36] observed an improvement in PA 12/GO tensile strength, as well as a slight increase in its plasticity. They also observed that impact strength increases up to 0.6 wt% GO content, and then decreases, due to filler agglomeration.

In our previous work, pure silica was used to improve the mechanical properties, thermal stability, chemical resistance, and flame retardancy of polyamide 6 [37]. Furthermore, water absorption was significantly reduced. The effect depended on the silica size and content.

Therefore, this article presents the effect of graphene oxide-modified silica and maleic anhydride (MAH) used as a compatibilizer on the structure, thermal, and mechanical properties of polyamide 6. The structure and thermal properties were analyzed by Attenuated total reflectance (ATR)-Fourier transformation infrared spectroscopy (FT-IR), scanning electron microscopy (SEM), dynamic thermomechanical analysis (DMTA), thermogravimetric thermal analysis (TGA), and differential scanning calorimetry (DSC). Moreover, water absorption, impact strength, and tensile properties were determined.

EXPERIMENTAL PART

Materials

Graphene oxide (GO) nanoplates used in this study were supplied by Sigma Aldrich (Darmstadt, Germany). Polyamide 6 (PA) was a Tarnamid T27 (MFR = 2.6 g/10 min at 230°C and 0.32 kg load), purchased from Azoty Tarnow Group (Poland). Graphene oxide-modified spherical silica (GO-SiO_2) were synthetized by the reported sol-gel process [38–40] and used at concentration of 1 wt%. The average diameter of the original silica was 30 and 60 nm. Maleic anhydride (MAH) with a molecular weight of 98.06 and melting point 54–56°C was supplied by Sigma Aldrich (Darmstadt, Germany), used at a concentration of 0.5 wt%.

Silica preparation

Graphene oxide-modified silica (GO-SiO_2) was synthesized using the procedure published elsewhere [38]. Briefly, ethyl alcohol, aqueous ammonia and distilled water were mixed, then TEOS (TES 28, Wacker Chemie, Germany) was added and stirred for 2 h, followed by graphene oxide was added to the reaction mixture and stirred for 1 h. The obtained silica sol was dried in an oven at 50–90°C for 2 h.

Composites preparation

Prior to mixing, PA was dried at 80°C to a moisture content of 0.01% (Somos TF10, Germany). PA was melting blended with 0.5 wt% MAH and reinforced with 1 wt% GO-SiO_2 using a Berstorff ZE-25x33D (D = 25 mm, L/D = 33) co-rotating twin-screw extruder under the following conditions: rotation speed 150 rpm, throughput 5 kg/h, extruder head temperature 235°C and barrel temperature 230–240°C, according to the procedure published elsewhere [41]. Separate gravimetric feeders were used for PA, MAH, and silica. Pure PA was processed under the same conditions as the nanocomposites to ensure the same thermomechanical history. Finally, standard dumb-bell samples (type 1A, ISO 527-2) with a thickness of 4 mm were injection molded at a temperature of 210–230°C, an injection pressure of 850 bar, a holding pressure of 350 bar, a mold temperature of 60°C and a cycle time of 18 s using an Arburg 420 M single-screw injection molding machine (Allrounder 1000-250, Germany) to obtain samples for SEM and mechanical tests. Prior to testing, specimens were dried for 72 h at 80°C in vacuum.

Methods

Silica characterization

Particle size and particle size distribution were measured by photon correlation spectroscopy (PCS), using a Malvern apparatus (Zetasizer Nano ZS). The morphology of graphene oxide-modified silica was studied using a Jeol JSM-6490LV (Japan) scanning electron microscope (SEM), operating at an accelerating voltage of 15 kV. The specific surface area and pore volume distribution of hybrid nanofillers were determined by low-temperature nitrogen adsorption using the TriStar II 3020 V1.03

apparatus from Micromeritics (USA). The studies were conducted at the nitrogen boiling point (–196°C). The Brunauera, Emmett and Teller (BET) theory were used to determine the specific surface area, and the pore volume distribution was calculated based on the adsorption isotherm using the Barrett-Joyner-Halenda (BJH) method.

Composites characterization

Attenuated total reflectance (ATR)-Fourier transformation infrared spectroscopy (FT-IR) was used for chemical structure analysis (Nicolet 6700 instrument,Thermo Electron Corporation, USA). The spectra were recorded using at least 32 scans with 4 cm^{-1} resolution, in the spectral range of 4000–400 cm^{-1}. A diamond crystal with a penetration depth of 1.7 μm was used for the tests. The morphology of the composites studies was performed by scanning electron microscopy (SEM) using a high-resolution scanning electron microscope JSM 6490 LV from JEOL. Thermal properties of the nanocomposites were studied by differential scanning calorimetry (DSC) using a Mettler Toledo DSC 822e. The samples were heated, cooled, and reheated at a rate of 10°C/min in the temperature range from 30°C to +240°C. The melting temperature (T_m) and crystallization temperature (T_c) were taken as the peak extremum of a given transformation. The degree of crystallinity (X_c) was calculated from the melting enthalpy results (ΔH_m) of each sample using Equation (1), where: ΔH_m and ΔH_0 are the enthalpies of fusion for composites and 100% crystalline PA6 (230 J/g), respectively [42].

$$X_c = \frac{\Delta H_m}{w_{PA6}\Delta H_0} \cdot 100 \quad (1)$$

Water absorption was determined according to ISO 62 standard – samples, after drying at 80°C for 6 h, were immersed for 48 h in distilled water, removed, dried from the top with tissue paper and weighed. An average weight of five samples was determined. Tensile properties were evaluated using an Instron 4505 testing machine according to the standard ISO 527-2. The crosshead speeds for tensile and tensile modulus tests were 5 and 1 mm/min, respectively. The gage length for tensile tests was 50 mm. Notched Charpy impact strength was assessed using a Zwick apparatus according to the ISO 179-1 (U) standard. All tests were conducted at room temperature. Minimum five measurements were done for each data point in all mechanical property tests. Dynamic mechanical thermal analysis (DMTA) was conducted on a Rheometrics RDS 2 dynamic analyzer (USA), with a specimen dimension of 63 × 11 × 4 mm, prepared by injection molding. Measurements were conducted in the temperature range from –150°C to 150°C with a vibration frequency of 1 Hz at a torsional strain of 0.1% and a heating rate of 3°C/min. The storage modulus (G') and loss angle tangent (tg δ) were determined. Prior to testing, specimens were dried for 72 h at 80°C in vacuum. Thermal stability was determined by thermogravimetric analysis (TGA) using a TGA/SDTA 851e thermogravimetric analyzer from Metler Toledo. The samples were heated at a rate of 10°C/min in the temperature range from +25 to +700°C in an air atmosphere. The temperature of 10% mass loss ($T_{10\%}$), the temperature of the maximum decomposition rate (T_{max}) and the total mass loss of the sample were determined.

RESULTS AND DISCUSSION

Synthetized GO-SiO_2 characterization

Figure 1 shows the particle size distribution of graphene oxide-modified silica (GO-SiO_2). The detailed characteristics of GO-SiO_2 are presented in Table 1. The developed process [38] allows to obtain a spherical shape, characterized by an almost uniform particle size distribution and ability to form tightly packed monolayers (Fig. 2).

Fig. 3 shows nitrogen adsorption and desorption isotherms at 77 K of GO- SiO_2 parameters differing in their useful value. The shape of type IV nitrogen adsorption/desorption isotherms and separate H2 type hysteresis are characteristic for the mesoporous structure.

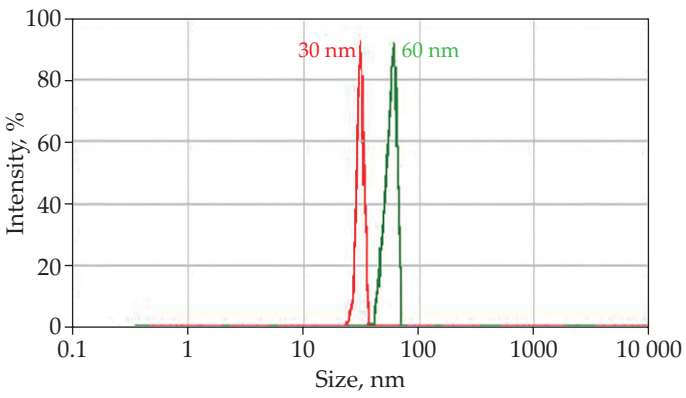

Fig. 1. Particle size distribution of GO-SiO_2 with an average size of 30 and 60 nm

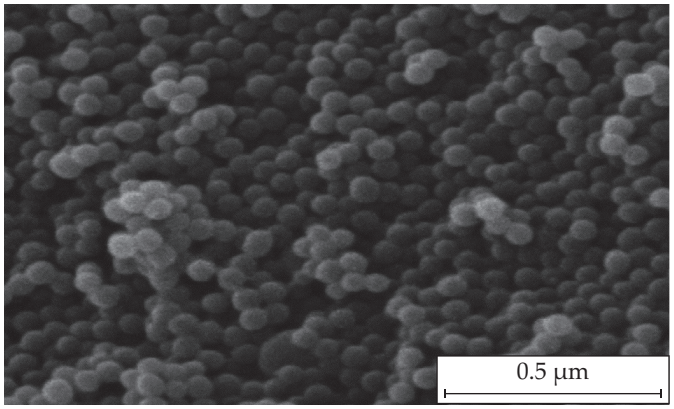

Fig. 2. SEM micrograph of GO-SiO_2 particles with an average size of 30 nm

T a b l e 1. GO-SiO_2 characteristic

Parameter	Average GO-SiO_2 size, nm	
	30	60
GO content, wt%	0.08	0.08
Thermal conductivity, W/m·K	0.888	0.099
Specific surface area, m^2/g	170.7	180.2
Mesopore volume, cm^3/g	0.4	0.4
Average pore size, nm	8.2	8.8

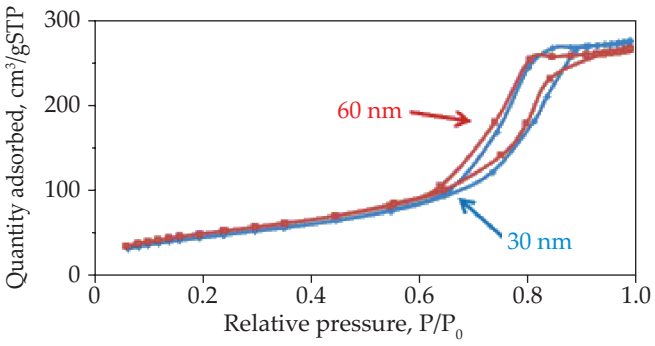

Fig. 3. Nitrogen adsorption and desorption isotherms at 77 K of GO-SiO_2

Chemical and morphological analysis of PA/GO-SiO_2 composites

Fig. 4 presents the FT-IR spectra of PA, GO-SiO_2, PA/GO-SiO_2 (99/1) and PA/GO-SiO_2/MAH (99/1/0.5) nanocomposites. The FT-IR spectrum of PA demonstrated a peak at 3291 cm^{-1} assigned to the N-H stretching, and two absorption peaks at 2930 and 2866 cm^{-1} corresponded to the methylene stretching vibration. Moreover, several sharp absorption peaks were observed at 1633, 1540, 1465, 1200, and 687 cm^{-1} attributed to amide-I (C=O stretching vibration), amide -II (C-N stretching and N-H bending vibration), amide-III (C-H in-of-plane bending vibration), amide-IV (C-CO stretching vibration) and amide-V (N-H out-of-plane bending vibration), respectively [43, 44]. The spectrum of GO-SiO_2 shows a broad peak with a maximum at 1050 cm^{-1} assigned to the Si–O and C–O–C vibrations originating from silica and GO, respectively. A shoulder with a maximum of 1255 cm^{-1} is also visible at this peak which can be assigned to Si–C and C–O bonds [45, 46]. Moreover, there are two peaks at 940 and 790 cm^{-1}, belonging to C–O and Si–C. The observed peaks confirm the incorporation of GO into the silica structure. The peaks at 1200 and 687 cm^{-1} indicate that both PA and PA/GO-SiO_2 nanocomposites exist in the α crystalline form. Moreover, a small band at 936 cm^{-1} appears in the spectra of PA and PA/GO-SiO_2, which corresponds to the γ-phase crystals of polyamide 6 [43]. It should be noted that the absorption peak at 936 cm^{-1} disappeared in the spectrum of PA/GO-SiO_2/MAH. Moreover, after the addition of GO-SiO_2, the intensity of N-H stretching (3291 cm^{-1}), methylene stretching (2930 and 2866 cm^{-1}), C=O stretching (1633 cm^{-1}) and C-N stretching and N-H bending (1540 cm^{-1}) peaks increased in

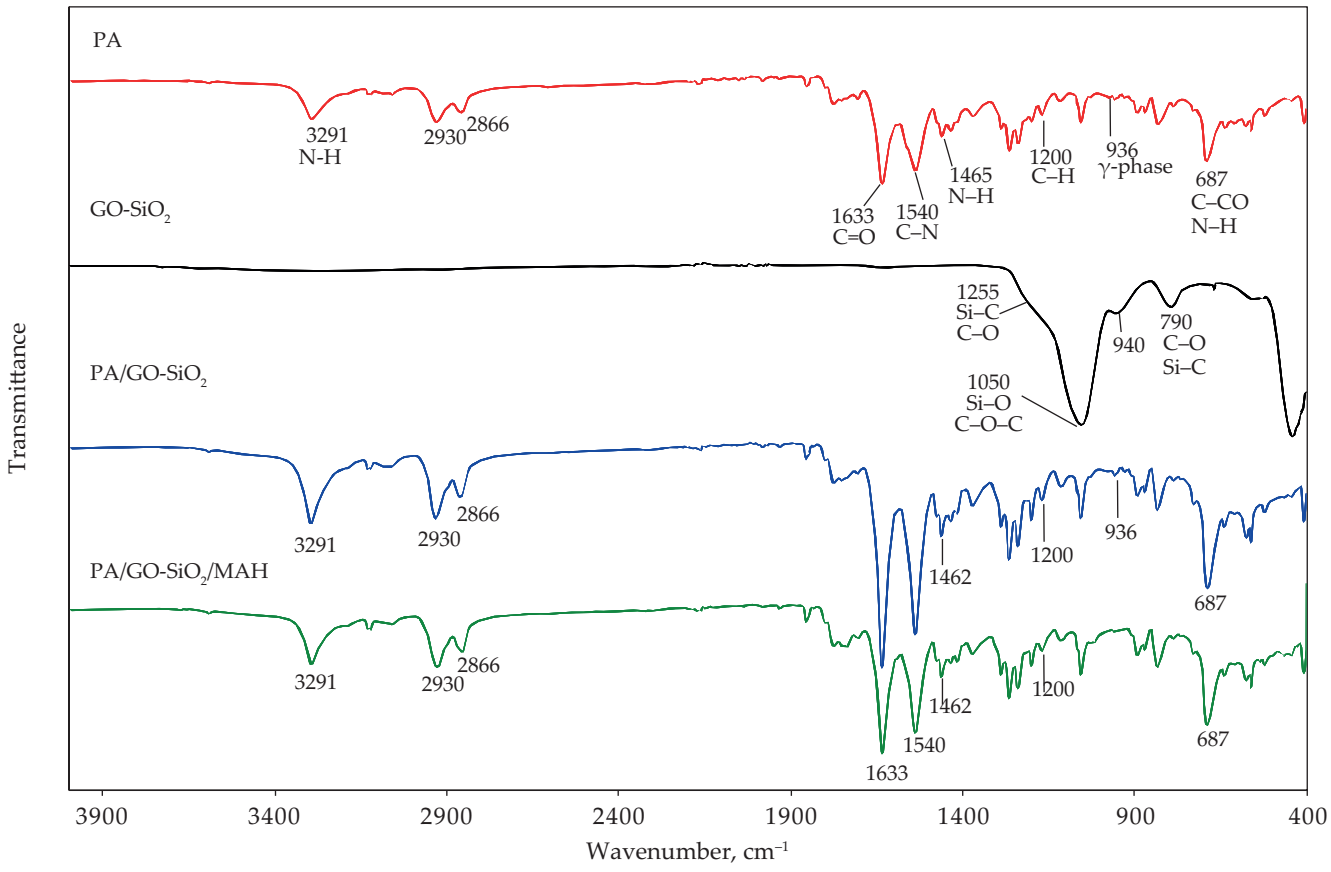

Fig. 4. FT-IR spectra of polyamide, GO-SiO_2 and PA/GO-SiO_2 nanocomposites

a) b)

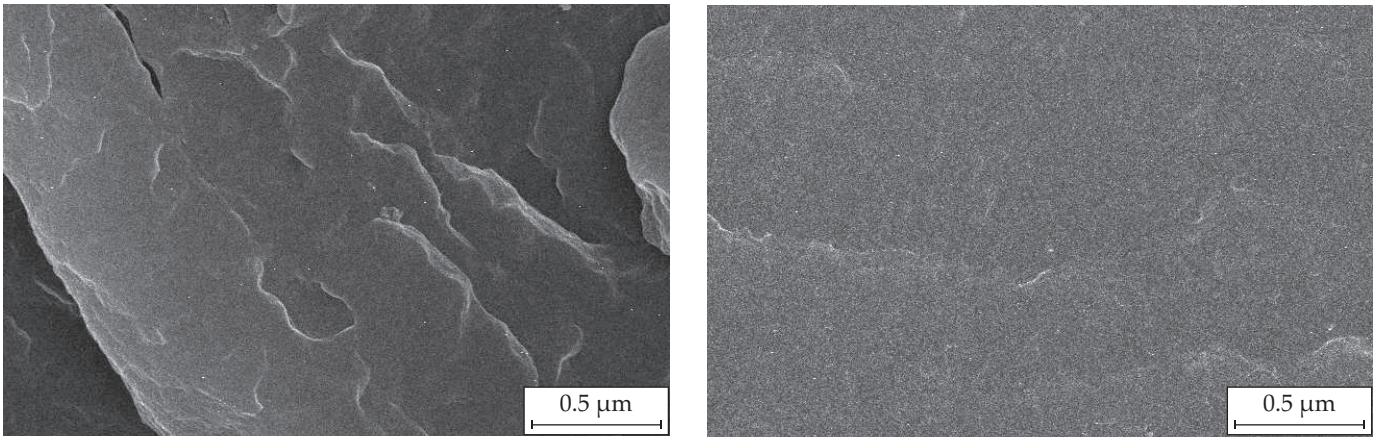

Fig. 5. SEM images of PA filled with 1 wt% GO- SiO_2 (30 nm): a) without MAH, b) 0.5 wt% MAH

a) b)

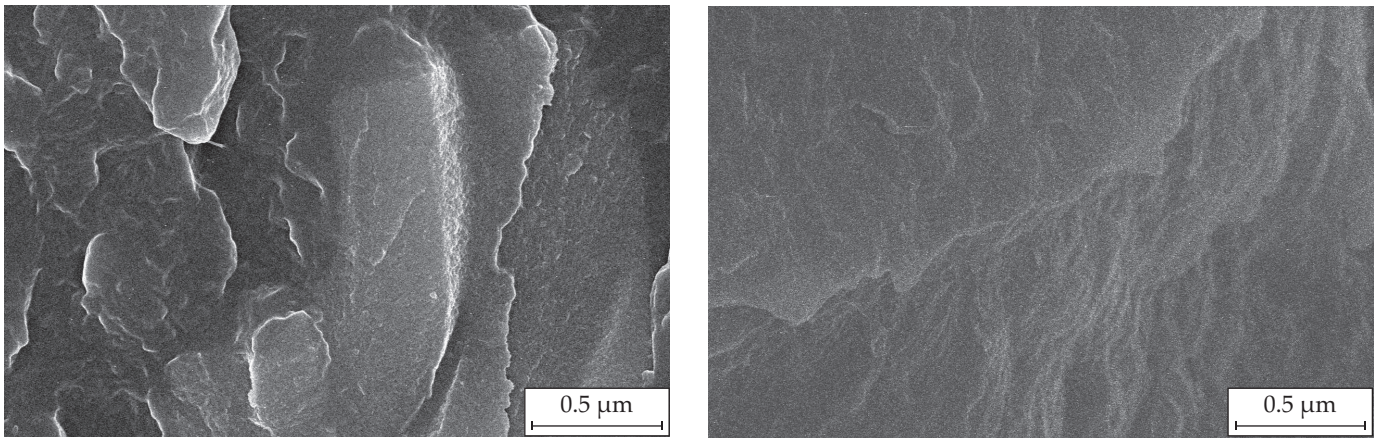

Fig. 6. SEM images of PA filled with 1 wt.% GO- SiO_2 (60 nm): a) without MAH, b) 0.5 wt% MAH

comparison to pure polyamide. On the other hand, the addition of MAH caused a decrease in the intensity of the above absorption peaks. These spectral changes suggest that the addition of GO-SiO_2 and MAH affects the crystallinity of the polyamide. The results are consistent with the other studies [43, 46].

The properties of polymer nanocomposites based on graphene are significantly dependent on the specific surface area, aspect ratio, dispersion and content of graphene and the interaction at the interface [32, 33, 35]. The cross-section images of PA/GO-SiO_2 and PA/GO-SiO_2/MAH composites with 1 wt% GO-SiO_2 (30 and 60 nm) are presented in Fig. 5 and Fig. 6, respectively. The structure of the composites is homogeneous, which may indicate uniform dispersion and good anchoring of the nanofiller in the polymer matrix. MAH increases homogeneity of the PA/GO-SiO_2 composite, which may suggest better interactions at the polymer-nanofiller interface and results in better mechanical properties. However, the above results indicate that the presence of GO-SiO_2 and MAH did not significantly affect the morphology and microstructure of PA. This can be ascribed to the fact that the amount of GO-SiO_2 and MAH used is low compared to that of the pure PA.

Crystallization behavior of PA/GO-SiO_2 composites

The crystalline structures of polyamides are related to many factors, such as thermal treatment, stress history and the presence of moisture, additives and nanofillers.

The crystalline structure of PA and PA/GO-SiO_2 composites were studied with DSC analysis. PA as a polymorphic material can crystallize in two major phases: γ- and α- crystalline forms [43]. In general, the α-form is thermodynamically stable, but the γ-form is kinetically favored. Table 2 and Fig. 7 show the DSC results of the pure polymer and composites. The crystallization temperature T_c, melting temperature T_m and crystallinity X_c of pure PA6 and composites were determined. The introduction of GO-SiO_2 nanofiller into the polyamide matrix increases the degree of crystallinity from 20.4% (pure PA) to 21.9% (GO-SiO_2; 30 nm). Addition of MAH and increasing the size of silica slightly reduces crystallinity, which suggests tendency of the hybrid nanofiller to nucleate the crystalli-

zation of polyamide. Moreover, when MAH is added, the mobility of PA molecules was reduced and consequently the crystallite growth was reduced. Polymer crystallization starts under conditions of significant supercooling of the plasticized material - at a temperature lower by about 30°C than T_m, which is associated with limited movements of long chains of macromolecules. No significant changes in the T_m value were observed in relation to pure polyamide. However, in the case of crystallization temperature, the increase was up to 3°C, which suggests that GO-SiO_2 acted as a nucleating agent [44]. In the case of PA and composites containing GO-SiO_2, a double melting peak appears. It can be attributed to the melting of γ- (214–215°C) and α-form crystallites (220–222°C). In the case of nanocomposites compatibilized with MAH, only one peak occurs in the temperature range (220–221°C), resulting from the melting of the α phase or the overlap of the melting curves of the α and g phase crystallites. The a and γ crystallites determine the higher stiffness of the polymer below and above the glass transition temperature, respectively. The presence of γ crystallites also affects the increase in HDT. Higher crystallinity (and polymorphism) can actively contribute to the improvement of the thermal-mechanical properties of PA nanocomposites. However, due to the slight changes in the degree of crystallinity (DSC studies), the increased stiffness of the polymer is caused by interactions at the polymer-filler interface, rather than by the change in the degree of crystallinity. The formed nanodomains of GO-SiO_2 particles restrict the mobility of polymer chains and strengthen the polymer by creating individual microstructures, which in turn create an inhomogeneous interfacial region, where filler particles interact with the polymer matrix. Based on these observations, it can be concluded that the adhesion at the interface increased in all tested nanocomposites. Similar crystallization behavior was reported for PA6/silica [37], PA6/POSS [43] and PA6/graphene oxide [47].

T a b l e 2. DSC results of PA and PA/GO-SiO_2 composites

Sample	T_c °C	T_{mg} °C	$T_{m\alpha}$ °C	X_c %
PA	188	214	222	20.4
GO-SiO_2 (30 nm)	190	215	221	21.9
GO-SiO_2 (60 nm)	191	215	221	21.2
GO-SiO_2 (30 nm)/MAH	191	–	221	19.6
GO-SiO_2 (60 nm)/MAH	188	–	220	18.7

Water absorption of PA/GO-SiO_2 composites

Table 3 summarizes water absorption and mechanical properties of PA 6 composites with graphene oxide-modified nanosilica of 30 and 60 nm particle size, obtained with and without maleic anhydride. The addition of GO-SiO_2 significantly decreased water absorption of polyamide (about 30%). This low water uptake capacity could be attributed to the increased number of non-polar aliphatic groups and reduced amide linkage density, which originated from hydrogen bonds with water molecules [44]. Furthermore, water absorption did not change significantly upon the addition of MAH. This characteristic could be a unique property for the PA/SiO_2/MAH composites regarding material properties, utilization, and storage.

Mechanical properties of PA/GO-SiO_2 composites

Fig. 8 provides the stress-strain curves of PA and PA/GO-SiO_2 composites. Pure polymer and composites with MAH showed a yield point followed by plastic deformation. Moreover Table 3 summarizes mechanical properties, including tensile modulus, tensile strength, elongation at break and impact strength. The addition of the hybrid nanofiller increases the stiffness of the poly-

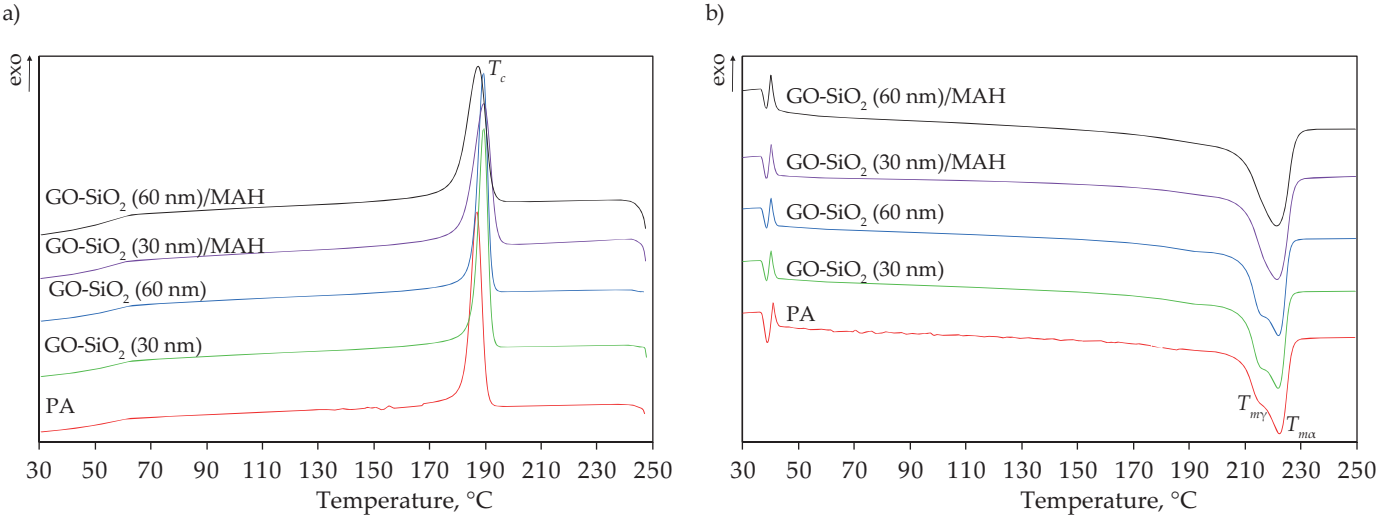

Fig. 7. DSC thermograms of PA and PA/GO-SiO_2 composites: a) cooling, b) 2^{ed} heating

T a b l e 3. Mechanical properties and water absorption of PA and PA/GO-SiO_2 composites; dried conditions

Sample	Tensile modulus MPa	Tensile strength MPa	Elongation at break %	Impact strength kJ/m²	Water absorption %
PA	2970±96	73±1	34±2.1	6±0.5	1.9
GO-SiO_2 (30 nm)	3310±47	71±1	8±0.4	5±0.5	1.2
GO-SiO_2 (60 nm)	3205±21	68±1	6±0.5	6±0.4	1.2
GO-SiO_2 (30 nm) /MAH	3570±38	75±1	31±2.0	6±0.3	1.3
GO-SiO_2 (60 nm) /MAH	3330±67	73±1	27±2.0	7±0.5	1.3

amide, as evidenced by the higher value of the tensile modulus of the composites. At the same time, the elongation at break decreases. On the other hand, the tensile strength and impact strength change only slightly. These properties depend on the size of the filler particle. GO-SiO_2 composites with smaller particle size are characterized by significantly lower tensile strength but lower impact strength. The effect of maleic anhydride depends on the size of the nanofiller particles. The highest tensile modulus is characteristic of the composite obtained from GO-SiO_2 with a particle size of 30 nm and MAH. In this case, tensile modulus was 20% higher compared to pure PA6. On the other hand, the composite containing GO-SiO_2 with a particle size of 60 nm and MAH is characterized by the highest impact strength, which is more than 10% higher compared to the pure polymer. Moreover, the addition of MAH caused a significant increase in the elongation at break, with a higher elongation being obtained in the case of a filler with a smaller particle size.

Dynamic mechanical properties of PA/GO-SiO_2 composites

The pure PA and the composites were subjected to DMTA under torsion mode, and loss tangent (tanδ) and storage modulus (G′) were investigated in relation to temperature, GO-SiO_2 size and the presence of MAH. The storage modulus of all samples (Fig. 9a) decreased with increasing temperature due to the softening and movement of polymer chains and segments at high temperature. The storage modulus indicates rigidity of the material. The decrease in modulus refers to the shift of materials from glass to rubbery state. Regarding the storage modulus at 23°C, the composites without MAH showed a slightly higher value compared to the pure polyamide 6.

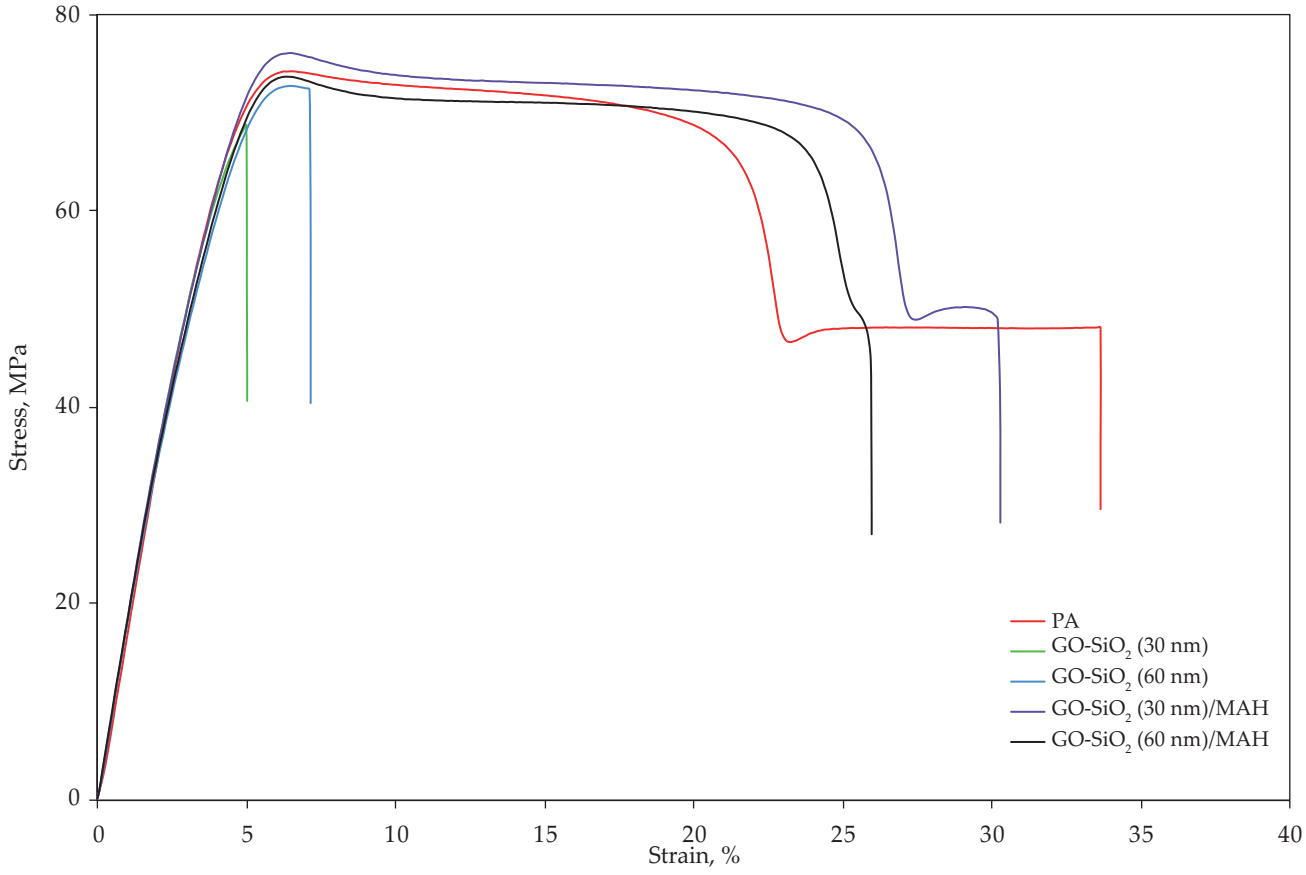

Fig. 8. Stress-strain curves of PA and PA/GO-SiO_2 composites

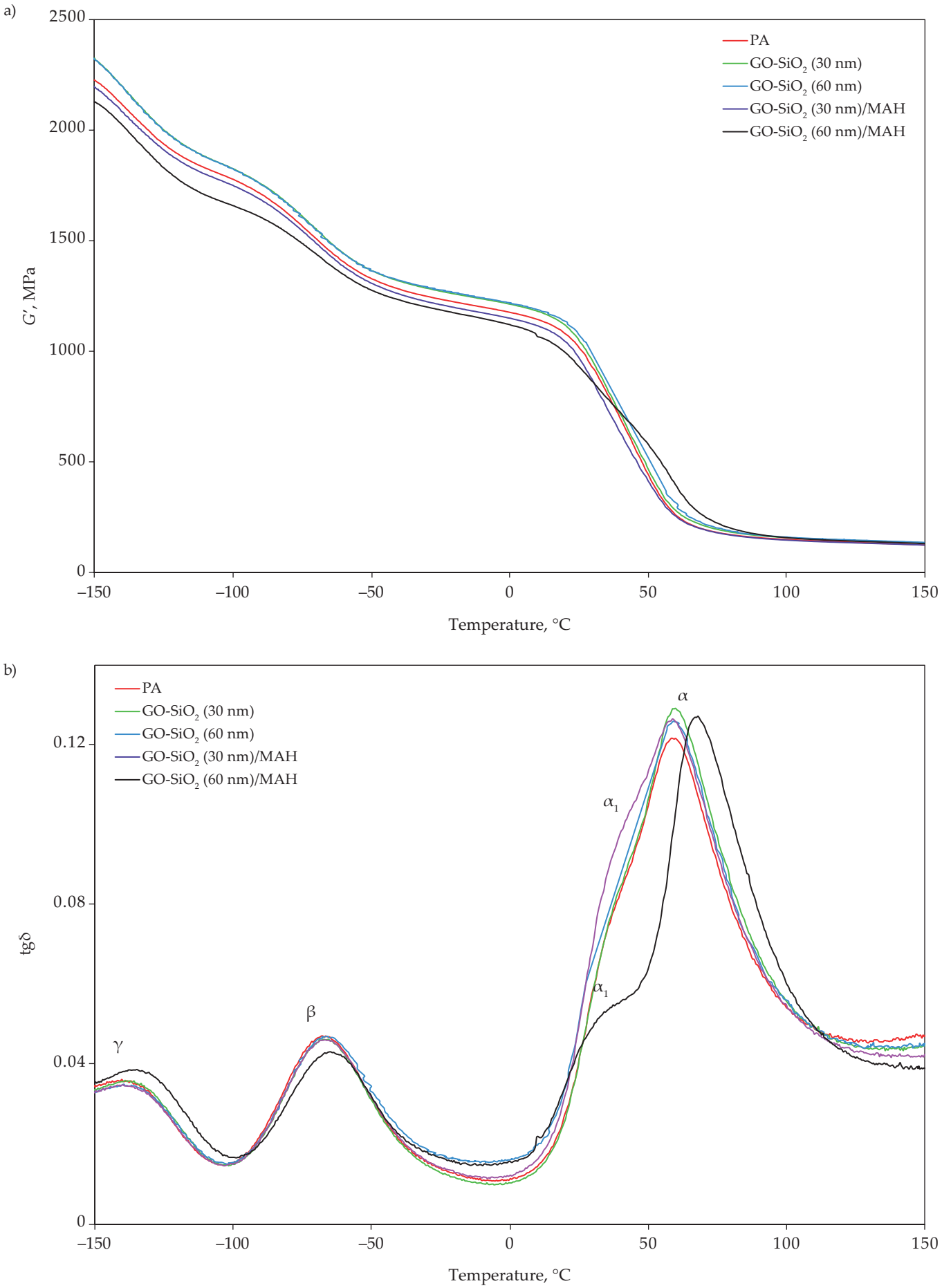

Fig. 9. DMTA plots of PA and PA/GO-SiO_2 composites: a) storage modulus, b) tgδ

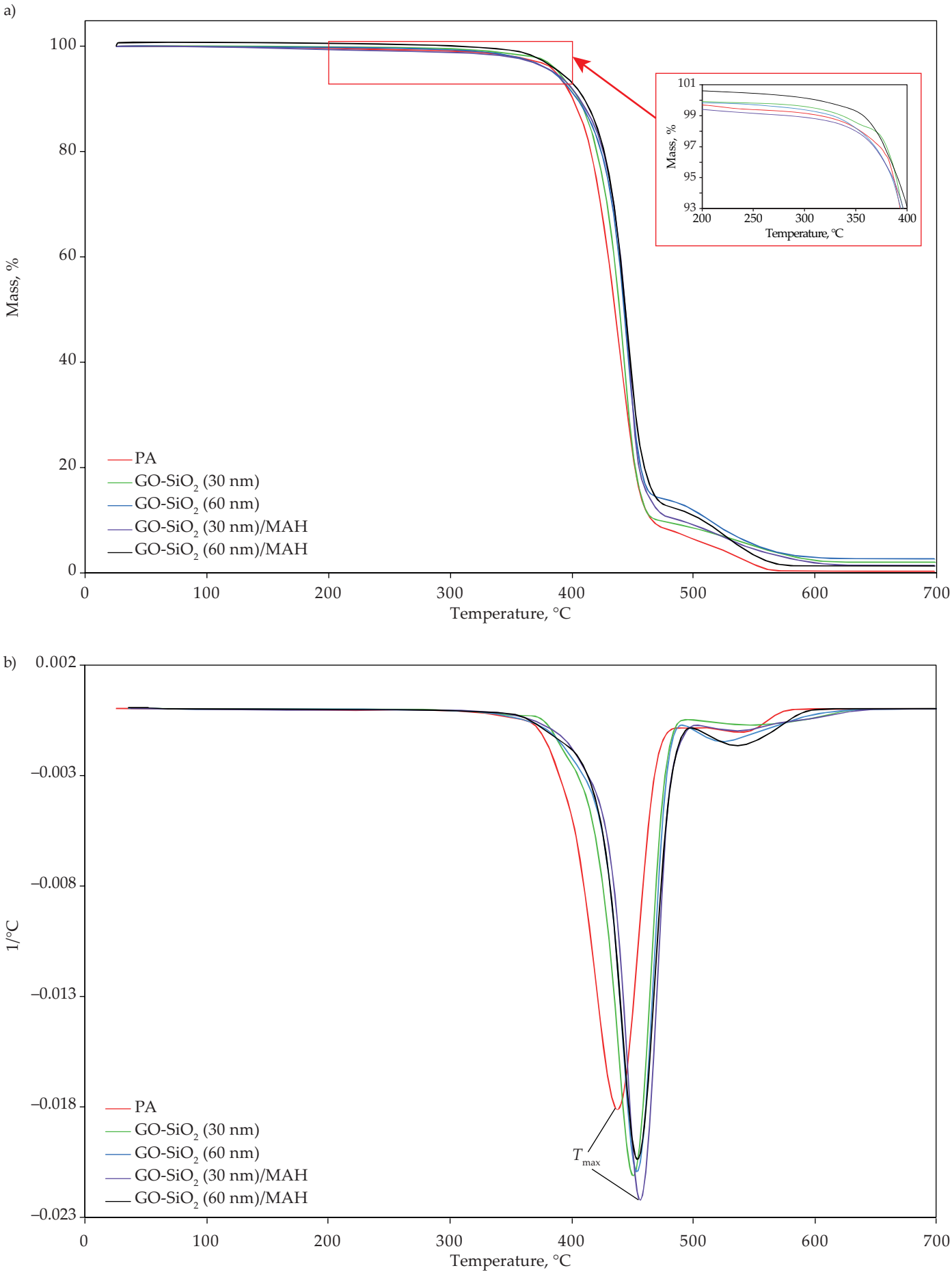

Fig. 10. TGA thermograms of PA and PA/GO-SiO_2 composites

T a b l e 4. DMTA data of PA and PA/GO-SiO$_2$ composites

Sample	G', MPa T = 23°C	Relaxation temperature, °C			
		α	α_1	β	g
PA	1060	59.3	–	–66.5	–137.0
GO-SiO$_2$ (30 nm)	1090	60.4	–	–67.0	–137.0
GO-SiO$_2$ (60 nm)	1110	60.5	–	–62.8	–134.0
GO-SiO$_2$ (30 nm)/ MAH	1000	60.9	40.1	–66.3	–139.7
GO-SiO$_2$ (60 nm)/ MAH	970	68.5	33.2	–63.5	–135.0

T a b l e 5. Thermal properties of PA and PA/GO-SiO$_2$ composites, determined by TGA

Sample	$T_{10\%}$ °C	T_{max} °C	Weight loss %
PA	404	448	99.75
GO-SiO$_2$ (30 nm)	407	458	98.00
GO-SiO$_2$ (60 nm)	405	462	97.40
GO-SiO$_2$ (30 nm)/MAH	404	468	98.70
GO-SiO$_2$ (60 nm)/MAH	410	466	98.70

However, the composite with larger silica size had the largest increase, reaching a value of 1110 MPa, suggesting a stronger interfacial bonding between PA and GO-SiO$_2$. Moreover, the addition of MAH causes a slight decrease in the storage modulus of the PA/GO-SiO$_2$ composites, which indicates lower stiffness.

Clear peaks were observed in the corresponding tgδ curves, indicating the occurrence of α, α1, β and γ relaxation transitions (Fig. 9b). The α relaxation transition is related to the glass transition temperature of PA. A shift in T_α was observed in PA/GO-SiO$_2$ composites, which is presented in Table 4. The composite containing larger GO-SiO$_2$ particles (60 nm) with the addition of MAH showed the most pronounced increase in T_α (about 9°C) compared to pure PA. The α_1 relaxation transition is visible in the composites, which is not present in pure polyamide; it is related to the presence of MAH and may indicate a change in the crystal structure of PA. The α_1 relaxation transition of composites containing GO-SiO$_2$ with a particle size of 30 nm occurs at a temperature of about 40°C, while for PA6 containing 60 nm GO-SiO$_2$ nanoparticles at a temperature of about 30°C. Nanosilica modified with graphene oxide also affects the temperature of the β and γ relaxation transitions. β relaxation is related to the mobility of polar amide groups not involved in hydrogen bonds with neighboring macromolecules and depends on the water content in the sample [43]. The g-relaxation is attributed to the movements of polar amide and methylene groups [48]. GO-SiO$_2$ with a particle size of 60 nm causes an increase in T_β and T_γ by 3–4 and 3°C, respectively. This indicates better dispersion of nanoparticles with dimensions of 60 than 30 nm. On the other hand, the use of a nanofiller with a smaller particle size has no effect on the value of the relaxation transition temperature. The only exception is the composite containing MAH, in which the T_γ temperature dropped by almost 3°C.

Thermal stability of PA and PA/GO-SiO$_2$ composites

Good thermal stability is of great importance for the practical applications of polyamides. Fig. 10 describes TGA/DTG curves of PA and PA/GO-SiO$_2$ composites, as measured by TGA under air atmosphere. Additionally, Table 5 presents the corresponding results, including decomposition temperature at 10% ($T_{10\%}$), temperature of maximum decomposition rate (T_{max}), and weight loss. All samples showed a similar weight loss trend, including a stable mass before 400°C followed by a complete decomposition between 450 and 600°C. The addition of graphene oxide-modified silica improves the thermal resistance of polyamide, as evidenced by 1–3°C higher $T_{10\%}$ and 10–14°C T_{max}. However, higher thermal resistance showed the composite with 60 nm nanosilica due to higher T_{max}. The addition of MAH further improves the thermal stability of PA. The composite containing smaller silica (30 nm) had lower $T_{10\%}$ but higher T_{max} compared to the composite with larger silica (60 nm). In addition, composites also have a higher (1–3°C) crystallization temperature and a higher degree of crystallinity. However, the effect of GO-SiO$_2$ on the crystallization of PA is small (see Table 2).

CONLUSIONS

Graphene oxide-modified silica nanocomposites based on polyamide 6 with maleic anhydride used as a compatibilizer were successfully obtained by melt extrusion in a twin-screw extruder. FT-IR, DSC and DMTA results suggest that the addition of GO-SiO$_2$ and MAH affects the crystallinity of the polyamide. Furthermore, GO-SiO$_2$ improved the stiffness of PA, with a greater effect being obtained for larger silica particles (60 nm). However, the addition of MAH slightly decreased stiffness compared to the neat polymer but improved the dispersion of the nanofiller as well as the interfacial interactions (SEM) resulted in better tensile properties and higher impact strength. Besides, GO-SiO$_2$ together with MAH significantly decreased water absorption (about 30%) and increased thermal resistance of polyamide due to higher $T_{10\%}$ (1–6°C) and T_{max} (10–20°C). The highest thermal resistance was observed in the composite containing smaller GO-SiO$_2$ particles (30 nm) and MAH.

The developed organic-inorganic polyamide composites with the properties of innovative engineering materials will enable the technological advancement of pro-

ducts to be raised and will stimulate new technological solutions in industries of strategic importance for the economy (e.g., electrical engineering, automotive, aviation, space science, construction).

Authors contribution

R.J. – conceptualization, supervision, methodology, validation, investigation, writing-original draft, writing--review and editing; A.S. – testing, methodology, validation, investigation; E.S-K. – testing, data curation, investigation; M.S. – testing, data curation, investigation; M.Ż. – testing, data curation, investigation; M.J. – testing.

Funding

This research received no external funding.

Conflict of interest

The authors declare no conflict of interest.

REFERENCES

[1] Compton O.C., An Z., Putz K.W. *et al.*: *Carbon* **2012**, *50(10)*, 3399. https://doi.org/10.1016/j.carbon.2012.01.061
[2] Dai Z., Li L., Zhang T.: *International Journal of Electrochemical Science* **2013**, *8(7)*, 9384. https://doi.org/10.1016/S1452-3981(23)12977-4
[3] Gómez-Navarro C., Burghard M., Kern K.: *Nano Letters* **2008**, *8(7)*, 2045. https://doi.org/10.1021/nl801384y
[4] Kulkarni D.D., Choi I., Singamaneni S.S. *et al.*: *ACS Nano* **2010**, *4(8)*, 4667. https://doi.org/10.1021/nn101204d
[5] Hu K., Gupta M.K., Kulkarni D.D. *et al.*: *Advanced Materials* **2013**, *25*, 2301. https://doi.org/10.1002/adma.201300179
[6] Li D., Müller M.B., Gilje S. *et al.*: *Nature Nanotechnology* **2008**, *3*, 101. https://doi.org/10.1038/nnano.2007.451
[7] Adamson A.W., Gast A.P.: "Physical chemistry of surfaces", John Wiley & Sons Inc., Michigan 1997. p. 777.
[8] Jiang L.Y., Huang Y., Jiang H. *et al.*: *Journal of the Mechanics and Physics of Solids* **2006**, *54(11)*, 2436. https://doi.org/10.1016/j.jmps.2006.04.009
[9] Shen B., Zhai W., Chen C. *et al.*: *ACS Applied Materials and Surfaces* **2011**, *3(8)*, 3103. https://doi.org/10.1021/am200612z
[10] Zhang H.L., Wei X.L., Zang Y. *et al.*: *Advanced Materials* **2013**, *25(30)*, 4097. https://doi.org/10.1002/adma.201300187
[11] Pei S., Cheng H.M.: *Carbon* **2012**, *50(9)*, 3210. https://doi.org/10.1016/j.carbon.2011.11.010
[12] Liu J., Fu S., Yuan B. *et al.*: *Journal of the American Chemical Society* **2010**, *132(21)*, 7279. https://doi.org/10.1021/ja100938r
[13] Cheng Q., Wu M., Li M. *et al.*: *Angewandte Chemie* **2013**, *125(13)*, 3838. https://doi.org/10.1002/ange.201210166
[14] Ramanathan T., Abdala A.A., Stankovich S. *et al.*: *Nature Technology* **2008**, *3*, 327. https://doi.org/10.1038/nnano.2008.96
[15] Kim W., Macosko C.W.: *Polymer* **2009**, *50(15)*, 3797. https://doi.org/10.1016/j.polymer.2009.05.038
[16] Wagner H.D., Vaia R.A.: *Materials Today* **2004**, *7(11)*, 38. https://doi.org/10.1016/S1369-7021(04)00507-3
[17] Moniruzzaman M., Winey K.I.: *Macromolecules* **2006**, *39(16)*, 5194. https://doi.org/10.1021/ma060733p
[18] Haque A., Ramasetty A.: *Composite Structures* **2005**, *71(1)*, 68. https://doi.org/10.1016/j.compstruct.2004.09.029
[19] Stankovich S., Dikin D.A., Dommett G.H.B. *et al.*: *Nature* **2006**, *442*, 282. https://doi.org/10.1038/nature04969
[20] Kim I.H., Jeong Y.G.: *Journal of Polymer Science Part B: Polymer Physics* **2010**, *48(8)*, 850. https://doi.org/10.1002/polb.21956
[21] Zhang H.B., Zheng W.G., Ya Q. *et al.*: *Polymer* **2010**, *51(5)*, 1191. https://doi.org/10.1016/j.polymer.2010.01.027
[22] Dasari A., Yu Z.Z., Mai Y.W.: *Polymer* **2009**, *50(16)*, 4112. https://doi.org/10.1016/j.polymer.2009.06.026
[23] Araby S., Zaman I., Meng Q. *et al.*: *Nanotechnology* **2013**, *24*, 165601. https://doi.org/10.1088/0957-4484/24/16/165601
[24] Steurer P., Wissert R., Thomann R. *et al.*: *Macromolecular Rapid Communications* **2009**, *30(4–5)*, 316. https://doi.org/10.1002/marc.200800754
[25] Yu K., Wang M., Qian K. *et al.*: *Fibers and Polymers* **2016**, *17*, 453. https://doi.org/10.1007/s12221-016-5862-8
[26] Ma Y., Di H., Yu Z. *et al.*: *Applied Surface Science* **2016**, *360(part B)*, 936. https://doi.org/10.1016/j.apsusc.2015.11.088
[27] Zhou X., Shi T.: *Applied Surface Science* **2012**, *259*, 566. https://doi.org/10.1016/j.apsusc.2012.06.113
[28] Sanjeev D.: *International Journal of Engineering Research and Technology* **2021**, *10(3)*, 533. https://doi.org/10.17577/ijertv10is030323
[29] Aneja K.S., Bohm S., Khanna A.S. *et al.*: *Nanoscale* **2015**, *7*, 17879.

https://doi.org/10.1039/c5nr04702a
[30] Baller J., Becker N., Ziehmer M. *et al*.: *Polymer* **2009**, *50(14)*, 3211. https://doi.org/10.1016/j.polymer.2009.05.020
[31] Ramezanzadeh B., Haeri Z., Ramezanzadeh B.: *Chemical Engineering Journal* **2016**, *303*, 511. https://doi.org/10.1016/j.cej.2016.06.028
[32] Pourhashem S., Vaezi M.R., Rashidi A.: *Surface and Coatings Technology* **2017**, *311*, 282. https://doi.org/10.1016/j.surfcoat.2017.01.013
[33] Yuan D., Wag B., Wang L. *et al*.: *Composites Part B: Engineering* **2013**, *55*, 215. https://doi.org/10.1016/j.compositesb.2013.05.055
[34] Jin J., Rafiq R., Gill Y.Q. *et al*.: *European Polymer Journal* **2013**, *49(9)*, 2617. https://doi.org/10.1016/j.eurpolymj.2013.06.004
[35] Pan Y.X., Yu Z.Z., Ou Y.C. *et al*.: *Journal of Polymer Science Part B: Polymer Physics* **2000**, *38(12)*, 1626. https://doi.org/10.1002/(SICI)1099-0488(20000615)38:12<1626::AID-POLB80>3.0.CO;2-R
[36] Rafiq R., Cai D., Jin J. *et al*.: *Carbon* **2010**, *48(15)*, 4309. https://doi.org/10.1016/j.carbon.2010.07.043
[37] Jeziórska R., Świerz-Motysia B., Zielecka M. *et al*.: *Polimery* **2009**, *54(10)*, 647.
[38] *Polish patent* 198 188 (2007).
[39] Jeziorska R., Świerz-Motysia B., Zielecka M. *et al*.: *Journal of Applied Polymer Science* **2012**, 125, 4326. https://doi.org/10.1002/app.36579
[40] Studziński M., Jeziorska R., Szadkowska A. *et al*.: *Polimery* **2014**, 59, 625. http://dx.doi.org/10.14314/polimery.2014.625
[41] *Polish patent* 242 257 (2022).
[42] Sinnokrot M.O., Valeev E.F., Sherrill C.D.: *Journal of the American Chemical Society* **2002**, *124(36)*, 10887. https://doi.org/10.1021/ja025896h
[43] Jeziórska R., Świerz-Motysia B., Szadkowska A. *et al*.: *Polimery* **2011**, *56(11-12)*, 804.
[44] Baniasadi H., Seppälä J.: *Materials Today Chemistry* **2021**, *20*, 100450. https://doi.org/10.1016/j.mtchem.2021.100450
[45] Kanta U., Thongpool V., Sangkhun W., Wongyao N., Wootthikanokkhan J.: *Journal of Nanomaterials* **2017**, *2017*, 2758294. https://doi.org/10.1155/2017/2758294
[46] Torres-Castillo C.S., Fuentes-Augustin J.E., Garcia-Reyes E.M. et al.: *Iranian Polymer Journal* **2023**, *32*, 139. https://doi.org/10.1007/s13726-022-01110-3
[47] Adel M., El-Shazly O., El-Wahidy E.W.F. et al.: *Polymer Engineering and Science* **2018**, *55*, 1201. https://doi.org/10.1002/pen.24683
[48] Ray S.S, Okamoto M.: *Progress in Polymer Science* **2003**, *28*, 1539. https://doi.org/10.1016/j.progpolymsci.2003.08.002

Received 17 X 2024.
Accepted 7XI 2024.